PCCP

RSC Publishing

PERSPECTIVE

View Article Online
View Journal | View Issue

Fill factor in organic solar cells

Cite this: *Phys. Chem. Chem. Phys.*, 2013, **15**, 8972

Boyuan Qi[ab] and Jizheng Wang*[a]

Received 2nd April 2013,
Accepted 2nd April 2013

DOI: 10.1039/c3cp51383a

www.rsc.org/pccp

The fill factor (FF) is an important parameter that determines the power conversion efficiency of an organic solar cell. There are several factors that can significantly influence FF, and these factors interact with each other very intricately. Due to this reason, a deep understanding of FF is quite difficult. Based on the three fundamental elements in the solar cell equivalent circuit, namely series resistance, shunt resistance and diode, we reviews the research progress in understanding on FF in organic solar cells. Physics lying behind the often-observed undesirable S-shaped *J–V* curves is also summarized. This paper aims to give a brief and comprehensive summary on FF from a fundamental point of view.

1 Introduction

The power conversion efficiency (PCE) of organic solar cells (OSCs) has been improved markedly in recent years and is now nearing the milestone value of 10%,[1–5] which makes its commercial industrialization very promising. The PCE of an OSC is determined by three important parameters, namely short-circuit current density (J_{SC}), open-circuit voltage (V_{OC}) and fill factor (FF). Fig. 1 shows a common current–voltage (*J–V*) curve for an OSC under dark and illumination. At a particular point in the *J–V* curve, the maximum power (P_m) is generated, with the current density and voltage marked as J_m and V_m, then the PCE can be calculated by:

$$\eta = \frac{P_m}{P_{in}} = \frac{J_m V_m}{P_{in}} = \frac{J_{SC} V_{OC} FF}{P_{in}} \quad (1)$$

where P_{in} is the light power incident on the device, and FF is expressed by:

$$FF = \frac{P_m}{J_{SC} V_{OC}} = \frac{J_m V_m}{J_{SC} V_{OC}} \quad (2)$$

FF characterizes how ''square'' the *J–V* curve is and it represents how ''difficult'' or how ''easy'' the photogenerated carriers can be extracted out of a photovoltaic device. The ideal value for FF is unity (100%), when the *J–V* curve is a rectangle. Only a small

[a] *Beijing National Laboratory for Molecular Sciences, Key Laboratory of Organic Solids, Institute of Chemistry, Chinese Academy of Sciences, Beijing 100190, P. R. China. E-mail: jizheng@iccas.ac.cn*
[b] *University of Chinese Academy of Sciences, Beijing 100049, P. R. China*

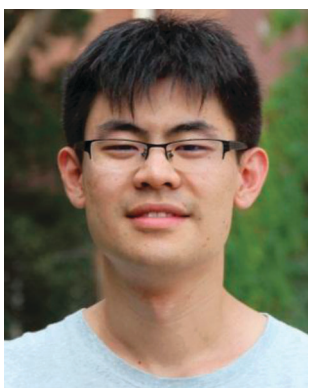

Boyuan Qi

Boyuan Qi received his BS degree from the Department of Physics at Nankai University in 2008 and obtained his MS degree from the Department of Physics at Peking University in 2011. He is now a PhD student at the Institute of Chemistry, Chinese Academy of Sciences. His research interests include device engineering and device physics in organic optoelectronics.

Jizheng Wang

Jizheng Wang got both his BS degree (1994) and MS degree (1997) from Lanzhou University and earned a PhD degree from the Institute of Semiconductors, Chinese Academy of Sciences (2001) in the area of inorganic electronics (III–V quantum well/dot lasers). He worked at the Cavendish Laboratory as a post-doc guided by Henning Sirringhaus and Richard H. Friend (2002–2005). He moved to US in 2005 and worked at Columbia University, Dupont and Arizona State University/US Army Flexible Display Centre. In 2010, he returned to the Chinese Academy of Sciences as a professor, and continues his research in organic electronics at the Institute of Chemistry.

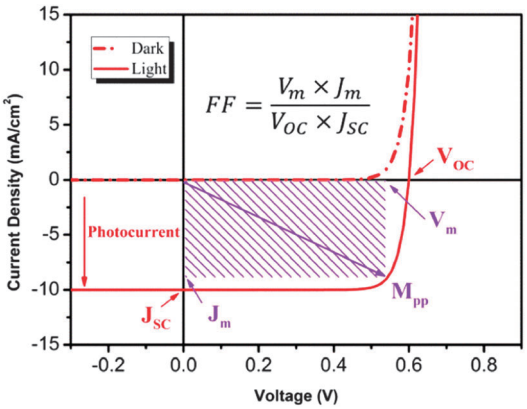

Fig. 1 Typical current–voltage characteristics for dark and light current in a solar cell illustrating the important parameters for such devices: J_{SC} is short-circuit current density, V_{OC} is open-circuit voltage, J_m and V_m are the current density and voltage at the maximum power point (M_{pp}), and FF is the fill factor.

voltage deviating from the V_{OC} ($< V_{OC}$) can make the current density rise perpendicularly to the maximum value (J_{SC}), and keep constant during the applied voltage changes from V_{OC} to zero and even a large reversed bias. In fact, FF cannot reach 100%. Even in the inorganic solar cells (the PCE of which is far larger than OSCs) the maximum FF reported is about 90%. While in OSCs, FF is usually in the range of only 50–70%. And if the space charge limited current (SCLC) dominates in the device, the FF cannot exceed 42%;[6,86,87] if the active area of the device is large, the collection efficiency of electrodes may be insufficient (usually the ITO side), then the FF will decrease with the increasing cell area, until the *J–V* curve deforms into a straight line which has a FF of 25%;[7,8] If there the interface is concerned (such as the interface between the electrodes and active layer, the interface between buffer layer and active layer, or the interface between donor and acceptor materials), an S-kink may occur in the *J–V* curve, and a serious S-kink can lower the FF to only *ca.* 10%.[9–11] Therefore, understanding of FF and the shape of *J–V* curve can be helpful to probe what is happening inside an OSC, especially when a new material is characterized. The *J–V* curve can give information on how this material works, such as: whether its energy level matches that of the active layer if this new material is a buffer layer, or whether its mobility is balanced with that of the acceptor (donor) material if it is a donor (acceptor) material. Then the feedback information can be instructive to the design of new materials in turn. However, FF is the least understood one among the three parameters that determine the PCE of OSCs. There are several factors that can influence the *J–V* curve and FF, and moreover these factors often interact with each other in a complex way. Generally in inorganic p–n junction solar cells, the equivalent circuit model is explored to describe the *J–V* characteristic of the device, which can fit the experimental data well. In this model, the behavior of the p–n junction is simulated by a diode, and the current losses (such as bulk resistances of materials and electrodes, or current leakage) can be modeled by series resistance (R_s) and shunt resistance (R_{sh}), respectively. Therefore the shape of the *J–V* curve and FF can be limited by the three elements in the equivalent circuit model. Based on this model, several empirical equations have been developed to express FF (including R_s and R_{sh}), and give high accuracies (better than a few percent).[12–16] Although there is no p–n junction in the OSCs, moreover, the fundamental mechanisms of the processes such as exciton generation, charge transfer and transport of carrier, are all different in OSCs, it is widespread proved that the equivalent circuit model is applicable to OSCs.[17–20] And the expressions for V_{OC} and FF deduced from inorganic solar cells hold true for OSCs. In this paper, we review the research progress of the factors influencing the *J–V* curve and FF in OSCs, and give a relatively clear picture of them on the basis of the equivalent circuit model. In the second part of this article, we introduce the equivalent circuit model for solar cells and some empirical equations of FF based on this model. In the third part of this paper, how the three elements (R_s, R_{sh} and diode) influence the FF and how they are limited by the internal mechanisms in OSCs is discussed. In OSCs an S-kink is frequently observed in the *J–V* curve, especially when a new material is characterized, in the fourth part of this paper, the causes of this phenomenon are summarized.

2 Equivalent circuit of solar cells and its relationship with FF

The equivalent circuit of ideal solar cells is shown in Fig. 2(a). The photo-generated current density J_{ph} is simulated by a constant current source which provides constant current under light illumination, the current flows in the device with applied voltage can be controlled by the diode. Within this circuit model, the shape of the *J–V* curve is determined only by the diode. It can be easily seen that the FF can approach 100% but can never reach 100% even in ideal solar cells because the *J–V*

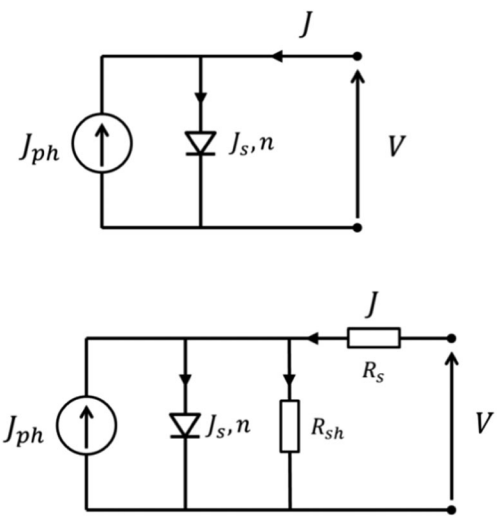

Fig. 2 Equivalent circuit for (a) ideal and (b) practical solar cells, J_{ph} is the photo-induced current density, J_d is the current density of the diode, R_s and R_{sh} are the series and shunt resistance, respectively, *J* is the current flow in the external load and *v* is the applied voltage.

curve of a diode cannot be rectangular. From the equivalent circuit, the *J–V* curve of ideal solar cells can be expressed by:

$$J(V) = J_S\left[\exp\left(\frac{qV}{k_BT}\right) - 1\right] - J_{ph} \quad (3)$$

where $J(V)$ is the recorded current density on the external load, J_S is the reverse saturation current density of the diode in the dark, q is the elementary charge, V is the applied voltage, k_B is the Boltzmann constant, T is the temperature and J_{ph} is the photo-generated current density. From this equation, the current density J can be expressed by a function with V as the argument, *i.e.* $J = J(V)$. Then the maximum output power of the solar cell can be calculated by $P_m = V_m \times J(V_m)$. It is reported in p–n junction solar cells that the V_m can be solved from the transcendental equation[13] as follows:

$$\left(1 + \frac{qV_m}{k_BT}\right)\exp\left(\frac{qV_m}{k_BT}\right) = \frac{J_{ph}}{J_S} + 1 \quad (4)$$

With the solution V_m substituting into eqn (4), J_m can be yielded, and then FF can be calculated by $V_mJ_m/V_{OC}J_{SC}$. The expression for FF explored in this way is really complicated, here we only introduce the result in the form of FF–v_{OC} curve in Fig. 3, where v_{OC} is the dimensionless voltage $v_{OC} = qV_{OC}/k_BT$. For simplicity, an approximation can be made which gives the well-known expression for FF:[14]

$$FF_0 = \frac{v_{OC} - \ln(v_{OC} + 0.72)}{v_{OC} + 1} \quad (5)$$

Here FF_0 is the fill factor of ideal solar cells (with no R_s and R_{sh}), and the accuracy of this expression is to one digit in the fourth significant place for $v_{OC} > 10$. If we take the common materials system used in OSCs, P3HT:PCBM, as an example, the V_{OC} of which is about 0.63 V, then the normalized v_{OC} is 24.23. According to eqn (5), the calculated FF_0 is 83.3%. However, in the literature, a common reported value for FF for P3HT:PCBM is about 65%. The large difference between the experimental value and calculated one from an ideal solar cell model implies that there must be other losses in the practical solar cells.

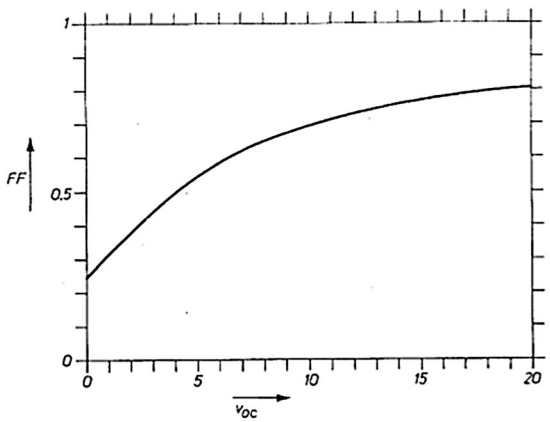

Fig. 3 The fill factor FF of an ideal solar cell as a function of the dimensionless open-circuit voltage $v_{OC} = qV_{OC}/k_BT$. Represented with permission from ref. 13. Copyright 1983, Elsevier.

In practical solar cells, parasite resistances are unavoidable factors. Therefore the series resistance and shunt resistance are introduced into the equivalent model to account for these energy losses (Fig. 2(b)). Usually, series resistance is derived from the bulk resistances of the active layer and electrodes, and the contact resistances between the active layer and electrodes. The shunt resistance originates from the current leakage induced by the pinhole in the cell, or the current leakage from the edge of the device. Taking the parasite resistances into consideration, the equivalent circuit equation can be expressed by:

$$J = J_S\left[\exp\left(\frac{e(V - JR_s)}{nk_BT}\right) - 1\right] + \frac{V - JR_s}{R_{sh}} - J_{ph} \quad (6)$$

According to eqn (6), the *J–V* curve of the solar cell is generally divided into three regions both in the dark and under illumination (Fig. 4).[21,22] Actually, if the photocurrent doesn't vary with the applied voltage, the *J–V* curve under illumination can be seen as the translational dark *J–V* curve (moved down by J_{ph}) From Fig. 4, it can be seen at negative voltages and low positive voltages (Region I), the *J–V* curve is a straight line with a slope determined by the $1/R_{sh}$; at intermediate positive voltages (Region II), the *J–V* curve is an exponential line (J depends exponentially on V), the characteristic of which is determined by the diode; and at high positive voltages (region III), the *J–V* curve is a second straight line with the slope controlled by $1/R_s$. It can be seen apparently that in Region III, if R_s becomes larger, the rise of J with increasing V will get slower ($1/R_s = dJ/dV$), then the slope of the *J–V* curve will decrease correspondingly, leading to less "squareness" of *J–V* curve, and a lower FF. Similarly, in Region I, if R_{sh} decreases, the slope of the *J–V* curve will increase. Then the *J–V* curve around J_{SC} becomes less parallel to the *x* axis, which will reduce the "squareness" of *J–V* curve and FF, too, while in region II, the *J–V* characteristic is determined by the diode. In practical solar cells, the *J–V* curve for diode can be represented by:

$$J = J_S[\exp(qV/nk_BT) - 1] \quad (7)$$

where n is the ideality factor of the diode. For ideal p–n junction Si solar cells, there are only diffusion currents that flow in the junction, so $n = 1$. If the currents in the device are dominated by recombination, then $n = 2$.[23] So in practical Si solar cells, where diffusion current and recombination current both exist, n is in the range of 1–2. After considering R_s, R_{sh} and n, the FF of p–n junction solar cell can be represented by:[12]

$$FF = FF_s\left(1 - \frac{v_{OC} + 0.7}{v_{OC}}\frac{FF_s}{r_{sh}}\right) \quad (8)$$

while

$$FF_s = FF_0(1 - 1.1r_s) + \frac{r_s^2}{5.4} \quad (9)$$

Here, FF_0 is the fill factor of ideal solar cells (eqn (5)), FF_s is the fill factor of solar cells that only have R_s, v_{OC} is the normalized open-circuit voltage which is expressed by V_{OC} divided by nk_BT/q instead of k_BT/q in eqn (5), r_s and r_{sh} are normalized resistances, which are the actual resistances R_s and R_{sh} divided

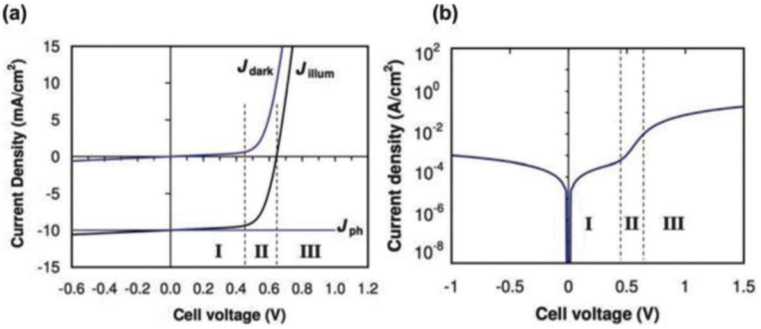

Fig. 4 (a) Typical *J–V* plot for an organic solar cell under dark and illumination. The three regions indicated account for where different effects dominate: Region I accounts for leakage (shunt) currents, Region II recombination currents, and Region III series resistance. (b) This *J–V* curve is from identical data as the blue (J_{dark}) curve in part (a), only presented on a semilog plot and using the absolute value of current density (negative current densities cannot be plotted on a log scale). Note that at $V = 0$, the dark current density = 0. Represented with permission from ref. 21. Copyright 2011, Royal Society of Chemistry.

by V_{OC}/J_{SC}, respectively. Other expressions for FF have also been reported by different research groups.[12–16]

All of these equations for FF are deduced from equivalent circuit model, and they can be applied in OSCs[24] because the *J–V* curve for OSCs can also be depicted by the equivalent circuit equation. However, it should be noted here that these equations for FF are empirical to some degree (which are summarized with the experimental results), and what they tell us about FF actually is quite obscure and limited. In the following part of this paper, how the parameters, R_s, R_{sh}, n and J_S (which are actually all factors that can affect FF) influence the FF and how these FF losses originate in OSCs will be introduced.

3 Factors that influence FF in OSCs

R_s, R_{sh} and diode have a competitive relation with each other in the equivalent circuit. Their interaction determines how the current flows in the device. R_s induces a voltage drop on itself, so it can divide the applied voltage from the diode. Therefore the larger the R_s is, the less voltage drop on the diode, which results in a slower increase of J with V, accordingly the less "square" the *J–V* curve becomes. R_{sh} has the effect of dividing current from diode, which makes it exhibit the opposite trend to that of R_s. When a reverse bias is applied, J should be small for the blocking effect of diode under reverse bias. However if R_{sh} is small, then the current under reverse bias will flow into R_{sh} and J will increase linearly with the increasing reverse voltage. This will also lower FF. In the following content of this section, how the three parameters influence FF is reviewed in details.

3.1 R_s

R_s is one of the important factors that limit the FF of solar cells.[25–29,91] It determines where the current mainly flows: to the diode or to the external load. We have explained it simply at the beginning of Section 3. Here a qualitative introduction on the basis of eqn (6) will be given. If R_s is small, $V - JR_s$ (potential drop on the diode) approaches V, then the major current of J_{ph} will flow into the diode; while if the R_s is large, $V - JR_s$ will be small, then the current of the diode is small. The majority of the J_{ph} will then flow into R_{sh} and R_s. Furthermore if the R_s is constant, the larger the J_{SC} is, the more pronounced the effect of the R_s is.[28] Because in eqn (8) and (9) the FF is the function of normalized resistance $r_s\left(\frac{R_s J_{SC}}{V_{OC}}\right)$, rather than the absolute value of R_s.

There are several methods to obtain the value of R_s in solar cells,[30,31] while in OSCs, the most common one is to take the slope of the *J–V* curve around V_{OC}. Generally R_s consists of (1) bulk resistance of the active layer and kinds of functional layers in the film, (2) bulk resistance of the electrodes, (3) contact resistance of every interface in the device and (4) probe resistance. In the fabrication of solar cells, reduction of R_s is one effective means to improve the performance of the device. It is reported that if the series resistance increases per 0.1 Ω, the FF of an inorganic solar cell declines about 2.5%.[32] In OSCs, a similar phenomenon could be observed. For example, in a planar heterojunction solar cell, copper phthalocyanine (CuPc) was used as donor material and C_{60} as acceptor material, a common efficiency of about 3.6% under 1.5 suns AM 1.5G simulated solar illumination was reported.[33] The FF of the device is 52% with the R_s of about 6.2 Ω cm^2, while Xue *et al.* improved the FF of this device to 60% by reducing the R_s to an ultra-low value of 0.1 Ω cm^2.[27] The authors also estimated the contributions of the four parts mentioned above to the overall R_s. In their experiment, the probe resistance is about 10 Ω, and the resistance of the electrodes is in the range of 4–15 Ω, the two resistance can be omitted when the device area (A) is smaller than 0.01 cm^2. And if the contacts between the electrodes and the active layer are Ohmic contacts and there are no large barriers at the interfaces between the organic layers in the device, the contact resistances can be negligible, too. Then the dominating contribution to the R_s is caused by the large resistivity of the organic layers. Here we can give a rough estimate of the resistivity according to eqn (10):

$$\rho = \frac{1}{\sigma} = \frac{1}{nq\mu} \tag{10}$$

Here, ρ is resistivity, σ is conductivity, n is the density of free carriers in organic films, q is the elementary charge and μ is carrier mobility. Taking the typical values in organic solar cells

here, n is about 10^{17} cm^{-3}, μ is about 10^{-3} cm^2 V^{-1} s^{-1}, so the calculated ρ is about 10^5 Ω cm. If the film thickness of the active layer is 100 nm, then the resistance of the active layer is $R = \rho\frac{l}{A} \times A = \rho \times l = 10^5\ \Omega\,\text{cm} \times 100\ \text{nm} = 1\ \Omega\ \text{cm}^2$. There are reports that by improving the mobility of carriers, R_s can be reduced and the efficiency of the devices is enhanced significantly.[11,34] And if the mobility is fixed, larger film thickness will lead to a larger R_s.[84,85]

However, the highest mobility of organic materials is still several orders of magnitude lower than their inorganic counterparts, so is there a large space for improving FF and the efficiency by improving the mobility? Or how further the FF and efficiency can be improved by optimizing R_s? In the work by Servaites *et al.*, they provide a means to answer this question.[28] They used the least-squares fit of eqn (6) to the actual experimental data, got the parameters in eqn (6) (*i.e.*, J_S, n, R_s, R_{sh}). Then they only changed the R_s in the equation and kept the other parameters constant, obtaining *J–V* curves with different R_s shown in Fig. 5.

It can be seen that the R_s of the test cell (1.4 Ω cm^2) is small enough, while further reduction of R_s to zero only leads to an efficiency improvement of 0.1%, and the FF also changes little. Enlarging R_s to 10 Ω cm^2 led to an obvious loss of FF and efficiency while the J_{SC} and V_{OC} remained unchanged. Further enlarging the R_s to 100 Ω cm^2, J_{SC}, the FF and efficiency all decreased significantly, only V_{OC} still remained unchanged. The change of FF and PCE with R_s is shown in Fig. 6. It can be seen that if R_s is smaller than 1 Ω cm^2, further reduction of R_s inducing improvement of FF is negligible. Therefore the mobility of the organic materials ($\sim 10^{-3}$ cm^2 V^{-1} s^{-1}) is sufficient enough for carrier transport, and the resulted R_s is already very small. So to further improve the mobility of organic materials to catch that of its inorganic counterparts is actually unnecessary.

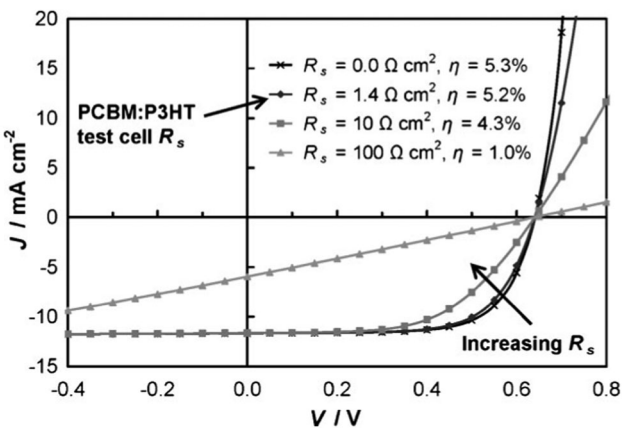

Fig. 5 The effect of R_s variation on projected *J–V* characteristics for the P3HT:PCBM test cell. These data assume that R_s is the only parameter that changes; all other parameters in eqn (5) are held constant (*i.e.* J_{ph}, R_{sh}, n and J_S). For the test cell, R_s = 1.4 Ω cm^2, and η = 5.2%. For a zero resistance cell (*i.e.*, R_s = 0), η increases by only 0.1 to 5.3%. Large R_s values ($\sim$100 Ω cm^2) have a significant effect on the cell efficiency (*e.g.*, an R_s of 100 Ω cm^2 reduces the cell efficiency to 1.0%). Represented with permission from ref. 28. Copyright 2010, Wiley-VCH.

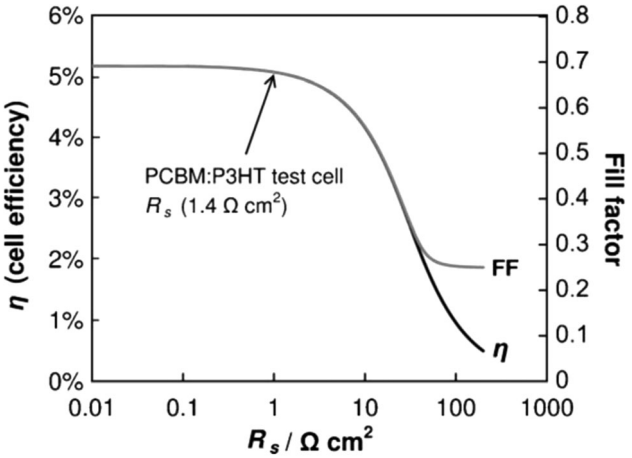

Fig. 6 Projected effect of R_s on the cell power conversion efficiency and FF for the P3HT:PCBM test cell. These data project how efficiency and FF would change as the cell resistance changes, with all other cell parameters in eqn (6) holding constant (*i.e.*, J_{ph}, R_{sh}, J_S and n). Note that the two curves are coincident until R_s approaches $\sim$50 Ω cm^2, at which point J_{SC} being also affected by R_s increases, thereby contributing to the efficiency losses. Represented with permission from ref. 28. Copyright 2010, Wiley-VCH.

Here are several points that should be noted:

(1) The above analysis is under the condition of mobility balance, if the mobility of holes and electrons don't match each other, then the carriers with lower mobility will accumulate in the device. It will lead to an additional electric field in the device, which blocks the extraction of the carriers, thus reducing the FF and efficiency. A serious unbalance of mobility will cause an S-shaped *J–V* curve and a very low FF of about 10%. More details on this aspect will be introduced in Section 4, S-shaped *J–V* curve.

(2) The contact resistance is left out of the consideration, because it is assumed that there are no adverse barriers, not only between the electrodes and the organic materials (Ohmic contact) but also at the interface of the active layer and functional layers. Adverse barriers can also cause S-shaped deformation in the *J–V* curve and will be discussed in Section 4, too.

(3) The other factors neglected above are the probe resistance and resistances of the electrodes, under the condition that the device area is smaller than 0.01 cm^2. However when the device area becomes larger, the effect of the two resistances cannot be neglected and can play an important role in R_s. According to $R = \rho\frac{l}{A}$, if ρ holds constant, when A increases, R will decrease. However this is only applied to the vertical resistance of the active layer and electrodes, while in the bulk electrode, the carriers firstly move in a vertical direction and then in a lateral direction so as to be collected finally by the probe. Because the cathodes are often high conductivity metals, the contribution of electrodes to R_s usually comes from ITO. Servaites *et al.* derived an equation that can describe the $R_{s,anode}$ well and concluded that if A increases, $R_{s,anode}$ will increase and dominate the R_s when A is large enough, and the vertical resistance in the device (originates from active layer, interfacial layer *etc.*) will keep constant regardless of A.[28] According to

eqn (6), when R_s is large, $V - R_sJ$ will be small, *i.e.* the voltage applied on the diode is small, so the current flowing in the diode is negligible, and then eqn (6) can be simplified to $J = \frac{V - JR_s}{R_{sh}} - J_{ph}$. It can be easily seen that the relationship between J and V under this condition is linear. By a simple mathematical derivation, an obvious conclusion can be obtained that the FF of a linear J–V curve (large area cells) is about 25% regardless of the value of J_{SC} and V_{OC}.

3.2 R_{sh}

Shunt resistance denotes the current losses in the cells, such as the current leakage from the edge of the cell, current leakage from the pinholes in the film or the current leakage by the traps. It has the effect of dividing the current in the equivalent circuit. Ideal R_{sh} should approach infinity, so current flows through R_{sh} is zero, *i.e.* there is no current leakage in the device. If R_{sh} is small, the current flowing through it cannot be neglected. Moreover, the current will change with the applied voltage, which makes the J–V curve deviate from "square" and thus lead to a lower FF.

The influence of R_{sh} to FF can be estimated by eqn (8). It is noted that generally in OSCs v_{OC} is around 15 (*e.g.* V_{OC} is about 0.6 V, n is about 1.5), which is far larger than 0.7, so $\frac{v_{OC} + 0.7}{v_{OC}}$ approaches 1. Then the term in the brackets is simplified to $1 - FF/r_{sh}$. It is known from calculations that if R_{sh} is larger than 6×10^3 Ω cm^2, the effect of R_{sh} on FF can be negligible. Tumbleston *et al.* proposed a method that can model the R_{sh} variation in the device with all the other parameters kept unchanged.[38] They used a variable external resistance load, R_{srE}, connected parallel to the device (with P3HT:PCBM as the active layer), to simulate the variation of R_{sh}. The R_{srE} could change from 0 Ω to 1×10^4 Ω, and the effect of R_{sh} on the J–V curve is shown in Fig. 7. It can be seen that the slope around J_{SC} changed obviously with decreasing R_{sh}, and led to lower FF.

Kim *et al.* studied the effects of design variables on the FF in OSCs with the familiar system of P3HT:PCBM.[26] They found that the thickness of the blend layer, the interface between the active layer and electrodes, and the illumination intensity are three variables that can influence R_{sh} and ultimately impact on FF.

When the layer thickness of the blend changed from 150 to 320 nm, the J_{SC} of the device was improved because of more light absorption in a thicker film. However, the R_{sh} of the device decreased obviously from 909 to 319 Ω cm^2, and FF decreased from 65 to 51%. With further increasing the thickness to 800 nm, all parameters of the device worsened, including J_{SC}, V_{OC}, R_s, R_{sh} and FF. The authors explained that in thick films, the charges need to travel a long distance before being collected by the electrodes, when the transit time is longer than the lifetime of the carriers, recombination will happen and lead to lower J_{SC} and larger R_{sh}.[95] Moreover, it is known widely that without a buffer layer (*e.g.* LiF, Ca), the Al atom will diffuse into the active layer and lead to a rough interface between the organic material and Al.[10,39] If the device is annealed thermally, the interfacial morphology can be improved. In this work, the authors found that R_s of the devices with and without thermal annealing are almost the same, while R_{sh} increased a lot after annealing. So the conclusion is that a good interfacial morphology can prevent current leakage and surface recombination. Finally, the relationship between illumination intensity and FF were explored. The authors found with the light intensity changing from 0.2 to 5 sun, the FF of the device varied from 61 to 34%. This is attributed to the reduction of R_{sh} from 1825 to only 33 Ω cm^2, because more recombination and current leakage occurred when there were more carriers in the device under high illumination intensity.

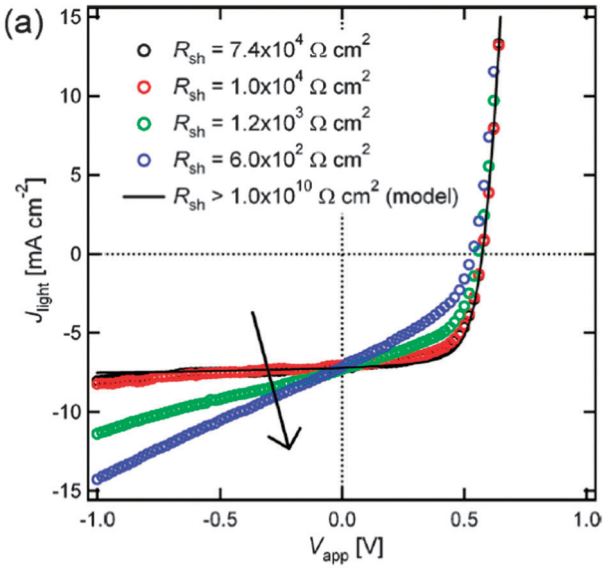

Fig. 7 J–V curve for P3HT:PCBM under 27 mW cm^{-2}, λ = 532 nm laser illumination with varying levels of R_{sh} as determined from the inverse slope of the J_{dark} curves at short-circuit. Arrows indicate decreasing R_{sh}. Represented with permission from ref. 38. Copyright 2010, American Institute of Physics.

The relationship between R_{sh} and the illumination intensity has been widely observed both in planar heterojunction small molecular OSCs and in bulk heterojunction polymer OSCs.[24,38,40,41] All results suggested an inverse linear relation between R_{sh} and P_0. In an equivalent circuit model, this was explained by the photoshunts, while in the drift/diffusion model (another model widely used in OSCs), the variation of J–V curve with the illumination intensity is attributed to the charge transfer (CT) state dissociation. Hence there should be a fundamental relation between the two models. Researchers modeled the CT state dissociation in the equivalent circuit by dividing the shunt resistance under illumination (R_{shL}) into two parts,[38,53] one is the shunt resistance in the dark (R_{sh}) which won't change with the illumination intensity, and the other one denotes the CT state dissociation (R_{shCT}).

$$R_{shL}^{-1} = R_{sh}^{-1} + R_{shCT}^{-1} \quad (11)$$

Here, the R_{shL} is obtained from the inverse slope of the J–V curve at short-circuit under illumination. Similarly, R_{sh} is taken as the inverse slope in the dark, and then the R_{shCT} can be calculated from eqn (11).

3.3 Diode

It was mentioned in the Introduction that Region II of the *J–V* curve is limited by the diode, the property of which can be characterized by eqn (7). At room temperature there are only two variables in eqn (7), n and J_S. n is dominated by the exciton dissociation and recombination in the device, and J_S is reported to be related to the difference between the highest occupied molecular orbital (HOMO) level of the donor material and the lowest unoccupied molecular orbital (LUMO) level of the acceptor material (*i.e.* ΔE_{DA}).[42–45] Therefore, the impact of the diode on FF is a result of the interaction between many factors.

The materials used in OSCs have a low dielectric constant ε, which is usually an order of magnitude lower than that of Si, so the Coulomb force of charge carriers is larger in OSCs than that in Si solar cells. This leads to a tightly binding hole–electron pair after light excitation rather than free charge carriers, and a donor–acceptor interface is needed to dissociate the exciton in OSCs. Light-electricity conversion goes through four processes: (1) photons are absorbed by the active layer and generate excitons; (2) excitons diffuse to the interface between donor and acceptor; (3) excitons dissociate into free holes and electrons at the donor/acceptor interface; (4) free carriers are transported in donor and acceptor materials and collected by the electrodes. The total efficiency that photons are converted to charge carriers can be expressed by the products of the efficiency of the four processes $\eta = \eta_A\eta_{ED}\eta_{CT}\eta_{CC}$, where η_A is absorption efficiency, η_{ED} is exciton dissociation efficiency, η_{CT} is charge transfer efficiency and η_{CC} is carrier collection efficiency. Generally η_{CT} and η_{CC} approach unity in many material systems. While in the process of exciton diffusion, recombination often happens, and even after exciton dissociation, electrons and holes may also have the possibility to recombine with each other, which is characterized by bimolecular recombination.[88–90] Therefore the possibility of recombination is larger in OSCs than in traditional inorganic crystal p–n junction solar cells, *i.e.*, the ideality factor n for OSCs is usually larger than that of inorganic crystal p–n junction solar cells. A solar cell with a lower n will have a larger FF than the solar cell with the same V_{OC} but a higher n because the FF increases with the normalized open-circuit voltage v_{OC} (v_{OC}/nk_BT) rather than the absolute value V_{OC} (shown in Fig. 3). Because n in OSCs is normally larger than that in inorganic solar cells, FF in OSCs is lower than that in inorganic solar cells, even OSCs usually own similar or even higher V_{OC}. For example, if a solar cell possesses a V_{OC} = 0.5 V, its FF_0 would be 80% when n = 1, but it will decline to 69% if n = 2.

According to the Shockley equation, the expression for V_{OC} can be calculated, which shows a good fit to the experimental results and is widely used in OSCs.

$$V_{OC} = \frac{nk_BT}{q}\ln\left(\frac{J_{SC}}{J_S}\right) \quad (12)$$

From eqn (12), v_{OC} can be calculated to be $\ln\left(\frac{J_{SC}}{J_S}\right)$, since FF is only determined by v_{OC} therefore it seems that FF is only limited by J_S (J_{SC} is about 10 mA cm^{-2} in many photovoltaic systems), which contradicts the previous conclusion that FF is influenced by n. However, Yoo *et al.* have found that both J_S and n increased with illumination intensity (*i.e.* they are different in the dark and under illumination).[24] So they modified the equivalent circuit to incorporate the change of n and J_S. The modified circuit has a second diode which accounts for the variation of J_S and n with light intensity, and a second parallel resistance accounting for the variation of R_{sh} with the light intensity which was discussed in the previous part. The modified equivalent circuit is shown in Fig. 8.

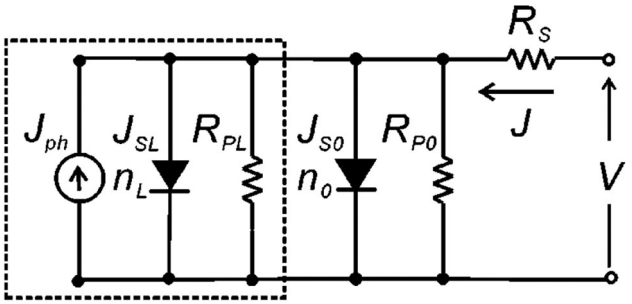

Fig. 8 Modified equivalent circuit containing an additional shunt resistance (R_L) and diode (J_{SL}, n_L) the parameters of which may be dependent on light intensity. Parameters with the subscript ''0'' indicate those obtained in the dark. Components with the intensity-dependent parameters are enclosed by the dashed line. Represented with permission from ref. 24. Copyright 2005, American Institute of Physics.

In eqn (12), the n and J_S are extracted by fitting eqn (6) to the *J–V* curve in the dark, so n and J_S should be n_0 and J_{S0} and kept constant regardless of light intensity. If n stands for the ideality factor under illumination, then v_{OC} can be expressed by:

$$v_{OC} = \frac{V_{OC}}{nk_BT/q} = \frac{(n_0k_BT/q)\ln\left(\frac{J_{SC}}{J_{S0}}\right)}{nk_BT/q} = \frac{n_0}{n}\ln\left(\frac{J_{SC}}{J_{S0}}\right) \quad (13)$$

From this equation, it can be seen FF is determined by the ideality factors in the dark and under illumination (n_0, n) and J_0.

Actually, there are two processes dominating n in OSCs. The first one is the exciton diffusion during which the geminate recombination happens; the second one is the charge collection during which bimolecular recombination and space charge effects may occur. Both processes could induce charge carriers' loss and enlarge the ideality factor n, thus reducing the FF.

De *et al.* have reported in alternating polyfluorene copolymer/fullerene blends the geminate recombination is the dominating loss mechanism which can be observed with transient absorption, while bimolecular recombination can be negligible.[46] In other words, the charge decay process has already happened before the exciton dissociation. Andersson and co-workers proposed if the Onsager–Braun model[81,82] is used to describe the charge transfer dissociation in these models, then increasing the mobility (even they are unbalanced) is always beneficial for the exciton dissociation, and thus leading to less current loss and higher FF.[47]

However Mandoc *et al.* proposed that within the Onsager–Braun model, if mobility reaches as high as 0.1 cm^2 V^{-1} s^{-1},

then the dissociation probability will approach 100% at the maximum power point (at which point the FF is calculated).[48] Furthermore, after the dissociation, there are still two mechanisms that influence the FF: transportation of carriers and bimolecular recombination, both of which are governed by the mobility of charge carriers. Increasing the mobility is beneficial to the exciton dissociation as well as carrier transport indeed, but on the other hand, high mobility would increase the current loss induced by bimolecular recombination, too.

It has been shown that the bimolecular recombination in OSCs is in the Langevin form.[49–51] The recombination rate can be written as:

$$R = \gamma(np - n_i p_i) \tag{14}$$

where $n(p)$ is the free electron (hole) density, n_i (p_i) is the intrinsic electron (hole) density, and γ is the recombination rate coefficient. The Langevin recombination rate coefficient is given by:

$$\gamma = \frac{q}{\varepsilon}(\mu_n + \mu_p) \tag{15}$$

where ε is the dielectric constant, $\mu_{n(p)}$ is the electron (hole) mobility. Langevin form gives the upper limit of the recombination constant. However, Deibel *et al.* found that this equation is only applicable to low mobility, at high mobility the bimolecular rate is mobility independent:[52]

$$\gamma = \begin{cases} \frac{q}{\varepsilon}(\mu_n + \mu_p), & \text{if } \frac{q}{\varepsilon}(\mu_n + \mu_p) \le \gamma_{crit} \\ \gamma_{crit}, & \text{if } \frac{q}{\varepsilon}(\mu_n + \mu_p) > \gamma_{crit} \end{cases} \tag{16}$$

The authors simulated the J_{SC}, V_{OC} and FF in OSCs with bimolecular recombination (eqn (14)) and Onsager–Braun dissociation, and found that FF increases with mobility firstly at low mobility, at moderate values (about 1×10^{-3}–1×10^{3} cm^2 V^{-1} s^{-1}), FF reaches a plateau, and decreases with a further increase of mobility. The increase of mobility accelerates the extraction of carriers and sweeps out almost all the carriers in the device, so the quasi-Fermi levels of electrons and holes get close to each other, which declines the V_{OC}. At low mobility, FF is limited by the transport of carriers, so it will increase with the mobility firstly, while at higher mobility, the extraction of carriers is unproblematic, then V_{OC} will be the determinant (FF will decrease with decreasing V_{OC} at high mobility). They also found the majority surface recombination (electrons cross the cathode and holes cross the anode interface) and minority surface recombination (electrons cross the anode and holes cross the cathode interface) play an important role in the balance of extraction and bimolecular recombination. The results discussed above are all based on the condition that both the majority and minority surface recombination rates are infinite, if the minority surface recombination rate could be confined to a low value, then the FF will saturate at its plateau and not decline with higher mobility.

In 2004, Riedel *et al.* studied the effect of temperature and illumination intensity on the electrical characteristics of polymer OSCs,[40] with the OC_1C_{10}-PPV:PCBM as the active layer (where OC_1C_{10}-PPV is poly[2-methoxy-5-(3.7-dimethyl octyloxy)-1,4-phenylene vinylene] and PCBM is phenyl-C_{61} butyric acid methyl ester). It was shown that when the temperature changed from 125 to 320 K, the R_s of the device increased from about 2 to more than 1000 Ω cm^2 in an exponential form. Similar observation has been reported in the small molecular OSCs (with $CuPc/C_{60}$ as the active layer),[41] where the authors proposed a fitting equation, $R_S \propto \exp(E_a/k_BT)$. With increasing T, carrier mobility increased, and as a result, the resistance decreased. Here E_a is an activation energy related to mobility. However, n and J_s have also been reported to increase with increasing T.[44,93] Therefore it is hard to predict how the FF changes with T, because it depends on the competing of R_s, J_s, n from the eqn (13).

Furthermore, space-charge formation in the device[6,86,87] (leading to FF < 42%), disorder in the organic materials[50] (influences recombination), energy difference of the LUMO (or HOMO) levels between donor and acceptor[21,53,54,92] (influences exciton dissociation) have also been studied and reported to be related to FF. Under different temperatures[73,93] and illumination intensities,[94] their effect on FF will vary concomitantly. Therefore a clear understanding of FF is quite complex.

4 S-shaped *J–V* curve

When characterizing new materials used for active layers or buffer layers in OSCs, S-shaped *J–V* curves are often observed in the experiments. The kink in the *J–V* curve usually appears in the fourth quadrant, *i.e.*, the power output region of the solar cells. The S-shaped *J–V* curve has been reported and researched by many groups.[9–11,55–63,83,97,98] There are many causes that can induce S-kinks, *e.g.* unbalance of charge carrier mobilities, defects or dipoles at the interface, energy barriers and low surface recombination rate of the cathode, *etc.* Although the causes of the S-kink appear quite different, the mechanism is in essence the same, *i.e.*there is carrier accumulation on the inside of the device, which alters the distribution of electric field inside the device.

Tress *et al.* proposed (based on their simulation data that in planar heterojunction solar cell) the S-kink will not show in the device with balanced mobility of holes and electrons, even if the mobility is very low, provided that the thickness of the donor layer and acceptor layer are the same. Lower mobility only induces a lower FF, however, the shape of the *J–V* curve is normal; while if the hole mobility is more than two orders of magnitude larger than electron mobility, the S-kink will appear in the *J–V* curve and *vice versa*.[11] This can be explained by analyzing the electric field distribution inside the device.

The carriers with lower mobility (take holes for example) can form space-charge in the donor material, then the potential drop on donor will be larger, and the electric field in the acceptor material will be smaller, in order to keep balanced carrier (electron *vs*. hole) extraction speed ($v = \mu E$). From Fig. 9, it can be seen around J_{SC}, the electric field in the device is large enough to guarantee satisfactory carrier extraction for both holes and electrons, so the *J–V* curve is similar to that with

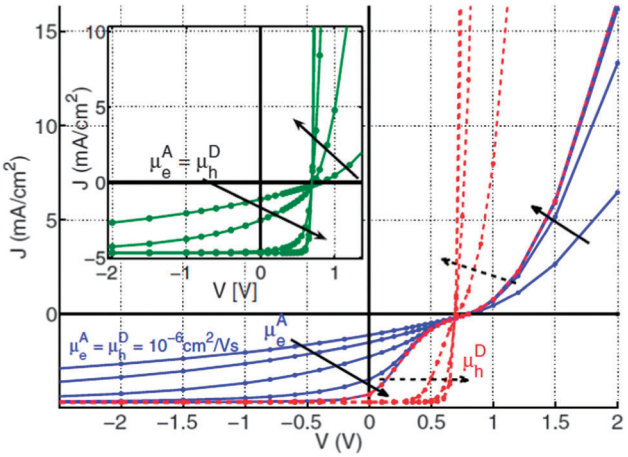

Fig. 9 Simulation data of a bilayer device with varied mobilities. Solid lines: hole mobility in donor μ_h^D kept constant at 10^{-6} cm^2 V^{-1} s^{-1}, with electron mobility in acceptor μ_e^A varied (10^{-6}, 10^{-5}, 10^{-4}, 10^{-3}, 10^{-2} cm^2 V^{-1} s^{-1}). Dashed lines: μ_e^A constant at 10^{-2} cm^2 V^{-1} s^{-1}, with μ_h^D varied 10^{-6}, ..., 10^{-2} cm^2 V^{-1} s^{-1}. Inset: balanced mobilities $\mu_e^A = \mu_h^D = 10^{-6}$, ..., 10^{-2} cm^2 V^{-1} s^{-1}. Represented with permission from ref. 11. Copyright 2011, American Institute of Physics.

balanced high mobility of carriers; while around V_{OC}, the electric field in the device is small, therefore the potential drop on the acceptor material is even smaller, when the electrons begin to pile up in the acceptor, leading to enhanced bimolecular recombination, then the *J–V* curve approaches the balanced low mobility one, thus a S-kink will appear in the *J–V* curve. The authors also verified the simulation with experimental results, by using donor and acceptor materials with different mobilities. Zhang *et al.* reported that if the layer with low mobility was doped to enhance the mobility of carriers, the S-kink would disappear.[57]

Furthermore, if the electrode has a low majority surface recombination rate, or there are large barriers in the device, the carriers will pile up at the interface, and induce an S-shaped *J–V* curve. This was produced not only by numerical simulation (with drift/diffusion model) but also by experimental results.[56]

Finally, the contact between the active layer and electrodes also play an important role in the properties of the *J–V* curve.[10,39] Maybe the most observed is the Al atom diffusing into organic materials when deposited directly onto the active layer without any buffer layer. This will lead to a bad interface morphology and induce defects in the active layer which makes the *J–V* curve change to an S-shaped one. Therefore cathode buffer layers are widely used when Al is explored as the cathode, both in polymer BHJ OSCs and in small molecules PHJ OSCs.

Although the causes of S-kink in *J–V* curve are different, one feature is the same, *i.e.*, carriers' accumulation in the device. The accumulated carriers induced an extra electric field which can block the same kind of carriers drifting to the electrode under the built-in potential. Therefore the additional electric field is in the direction opposite to the built-in potential and equidirectional to the applied voltage in the fourth quadrant. When the extra electric field plus the applied voltage equals the built-in electric field, it seems that the V_{OC} point is arrived at earlier. And from this point the current density will be low until the applied voltage is truly the same as V_{OC}, after which the injection behavior dominates in the device. So the *J–V* curve will show an S-shape characteristic in the fourth quadrant.

5 Conclusions

As one of the three important parameters that determine the efficiency of OSCs, FF can be influenced by many factors, which interplay with each other intricately. This makes FF the least understood one in OSCs, comparing to that of V_{oc} and J_{sc}. Based on the three equivalent circuit elements, namely R_s, R_{sh} and diode, we reviewed the present understanding on FF. R_s has a pronounced effect on the shape of *J–V* curve around V_{OC}, large R_s can divide the voltage from the diode, leading to a slower rise of *J* with increasing positive *V*, *i.e.*, the *J–V* curve becomes less "square" and FF decreases. R_{sh} governs the shape of the *J–V* curve around J_{SC}, small R_{sh} divides the current from J_{ph}, leading to *J* increasing with the reverse bias, *i.e.*, the *J–V* curve becomes less "square" and FF decreases as well. The properties of the diode determine the curvature of the *J–V* curve around the maximum power point. Carriers extraction and recombination are the main competing processes which are all governed by the mobility of carriers in the diode. High mobility is beneficial for the exciton dissociation and transport of carriers, but as a result, the recombination is enhanced, too. Therefore there is an optimized value of mobility, at which FF can be maximum. However, if the minority surface recombination rate can be limited (for example, keep Ohmic contact between electrodes and the active layer), the FF can maintain the maximum value with further increasing mobility. Moreover, the frequently observed S-shaped *J–V* curves during the characterization of devices are summarized in this paper. Generally there are four causes for the S-kink in the *J–V* curve: unbalanced mobility of hole and electron, bad interfacial morphology between the electrodes and the active layer (leading to low minority surface recombination), dipole and large barriers in the device. However the essential reason is the same, *i.e.* charge accumulation in the device, which introduces an additional electric field. The extra electric field can offset a portion of the built-in potential, leading to less efficient exciton dissociation and extraction of the carriers around the maximum power point, thus the *J–V* curve nearby becomes concave. Commonly, in the fabrication of OSCs, choosing proper buffer layers can help diminish the contact resistance (reduce R_s) or the current leakage (enlarge R_{sh}),[35,64–68] using an exciton blocking layer may reduce recombination,[55,63,69,70] enhancing the crystallinity of organic materials,[71,72] changing the molecular weight[36,74,75] and stoichiometry[76,77] of donor and acceptor, and improving the morphology[37,78–80,96] are beneficial for enhancing the mobility, and ultimately improving the FF, and hence the efficiency.

Acknowledgements

The authors acknowledge financial support from the National Natural Science Foundation of China (Grant Nos. 61072014 and 21021091), 973 Program (Grant No. 2011CB932304) and Hundred-Talent Program of Chinese Academy of Sciences.

References

1 T. Yang, M. Wang, C. Duan, X. Hu, L. Huang, J. Peng, F. Huang and X. Gong, *Energy Environ. Sci.*, 2012, **5**, 8208.
2 X. Li, W. C. H. Choy, L. Huo, F. Xie, W. E. I. Sha, B. Ding, X. Guo, Y. Li, J. Hou, J. You and Y. Yang, *Adv. Mater.*, 2012, **24**, 3046.
3 Z. He, C. Zhong, X. Huang, W.-Y. Wong, H. Wu, L. Chen, S. Su and Y. Cao, *Adv. Mater.*, 2011, **23**, 4636.
4 Z. He, C. Zhong, S. Shu, M. Xu, H. Wu and Y. Cao, *Nat. Photonics*, 2012, **6**, 591.
5 L. Dou, J. You, J. Yang, C.-C. Chen, Y. He, S. Murase, T. Moriarty, K. Emery, G. Li and Y. Yang, *Nat. Photonics*, 2012, **6**, 180.
6 V. D. Mihailetchi, J. Wildeman and P. W. M. Blom, *Phys. Rev. Lett.*, 2005, **94**, 126602.
7 W.-I. Jeong, J. Lee, S.-Y. Park, J.-W. Kang and J.-J. Kim, *Adv. Funct. Mater.*, 2011, **21**, 343.
8 D. Gupta, M. Bag and K. S. Narayan, *Appl. Phys. Lett.*, 2008, **93**, 163301.
9 G. del Pozo, B. Romero and B. Arredondo, *Sol. Energy Mater. Sol. Cells*, 2012, **104**, 81.
10 D. Gupta, M. Bag and K. S. Narayan, *Appl. Phys. Lett.*, 2008, **92**, 093301.
11 W. Tress, A. Petrich, M. Hummert, M. Hein, K. Leo and M. Riede, *Appl. Phys. Lett.*, 2011, **98**, 063301.
12 M. A. Green, *Sol. Cells*, 1982, **7**, 337.
13 A. de Vos, *Sol. Cells*, 1983, **8**, 283.
14 M. A. Green, *Solid-State Electron.*, 1981, **24**, 788.
15 E. Sánchez and G. L. Araújo, *Sol. Cells*, 1987, **20**, 1.
16 K. Taretto, M. Soldera and M. Troviano, *Prog. Photovoltaics*, 2012, **20**, 2325.
17 W. U. Huynh, J. J. Dittmer, N. Teclemariam, D. J. Milliron and A. P. Alivisatos, *Phys. Rev. B: Condens. Matter*, 2003, **67**, 115326.
18 P. Schilinsky, C. Waldauf, J. Hauch and C. J. Brabec, *J. Appl. Phys.*, 2004, **95**, 2816.
19 J. Rostalski and D. Meissner, *Sol. Energy Mater. Sol. Cells*, 2000, **63**, 37.
20 C. J. Brabec, S. E. Shaheen, C. Winder, N. S. Sariciftci and P. Denk, *Appl. Phys. Lett.*, 2002, **80**, 1288.
21 J. D. Servaites, M. A. Ratner and T. J. Marks, *Energy Environ. Sci.*, 2011, **4**, 4410.
22 C. Waldauf, M. C. Scharber, P. Schilinsky, J. A. Hauch and C. J. Brabec, *J. Appl. Phys.*, 2006, **99**, 104503.
23 S. M. Sze, *Physics of Semiconductor Devices*, Wiley, New York, 1981.
24 S. Yoo, B. Domercq and B. Kippelen, *J. Appl. Phys.*, 2005, **97**, 103706.
25 U. Rau, P. O. Grabitz and J. H. Werner, *Appl. Phys. Lett.*, 2004, **85**, 6010.
26 M.-S. Kim, B.-G. Kim and J. Kim, *ACS Appl. Mater. Interfaces*, 2009, **1**, 1264.
27 J. Xue, S. Uchida, B. P. Rand and S. R. Forrest, *Appl. Phys. Lett.*, 2004, **84**, 3013.
28 J. D. Servaites, S. Yeganeh, T. J. Marks and M. A. Ratner, *Adv. Funct. Mater.*, 2010, **20**, 97.
29 R. A. Street, K. W. Song and S. Cowan, *Org. Electron.*, 2011, **12**, 244.
30 M.-K. Lee, J.-C. Wang, S.-F. Horng and H.-F. Meng, *Sol. Energy Mater. Sol. Cells*, 2010, **94**, 578.
31 D. Pysch, A. Mette and S. W. Glunz, *Sol. Energy Mater. Sol. Cells*, 2007, **91**, 1698.
32 J. Lindmayer, *COMSAT. Tech. Rev.*, 1973, **3**, 1.
33 P. Peumans and S. R. Forrest, *Appl. Phys. Lett.*, 2001, **79**, 126.
34 Y. Zhang, J. Yu, J. Huang, R. Jiang and G. Huang, *J. Phys. D: Appl. Phys.*, 2012, **45**, 175101.
35 J. Yu, Y. Zang, H. Li and J. Huang, *Thin Solid Films*, 2012, **520**, 6653.
36 K. Tajima, Y. Suzuki and K. Hashimoto, *J. Phys. Chem. C*, 2008, **112**, 8507.
37 P. Vanlaeke, A. Swinnen, I. Haeldermans, G. Vanhoyland, T. Aernouts, D. Cheyns, C. Deibel, J. D'Haen, P. Heremans, J. Poortmans and J. V. Manca, *Sol. Energy Mater. Sol. Cells*, 2006, **90**, 2150.
38 J. R. Tumbleston, D.-H. Ko, E. T. Samulski and R. Lopez, *J. Appl. Phys.*, 2010, **108**, 084514.
39 D. Gupta, S. Mukhopadhyay and K. S. Narayan, *Sol. Energy Mater. Sol. Cells*, 2010, **94**, 1309.
40 I. Riedel, J. Parisi, V. Dyakonov, L. Lutsen, D. Vanderzande and J. C. Hummelen, *Adv. Funct. Mater.*, 2004, **14**, 38.
41 B. P. Rand, D. P. Burk and S. R. Forrest, *Phys. Rev. B: Condens. Matter Mater. Phys.*, 2007, **75**, 115327.
42 W. J. Potscavage Jr, S. Yoo and B. Kippelen, *Appl. Phys. Lett.*, 2008, **93**, 193308.
43 N. C. Giebink, G. P. Wiederrecht, M. R. Wasielewski and S. R. Forrest, *Phys. Rev. B: Condens. Matter Mater. Phys.*, 2010, **82**, 155305.
44 J. C. Nolasco, A. Sánchez-Díaz, R. Cabré, J. Ferré-Borrull, L. F. Marsal, E. Palomares and J. Pallarès, *Appl. Phys. Lett.*, 2010, **97**, 013305.
45 M. D. Perez, C. Borek, S. R. Forrest and M. E. Thompson, *J. Am. Chem. Soc.*, 2009, **131**, 9281.
46 S. De, T. Pascher, M. Maiti, K. G. Jespersen, T. Kesti, F. Zhang, O. Inganäs, A. Yartsev and V. Sundström, *J. Am. Chem. Soc.*, 2007, **129**, 8466.
47 L. M. Andersson, C. Müller, B. H. Badada, F. Zhang, U. Würfel and O. Inganäs, *J. Appl. Phys.*, 2011, **110**, 024509.
48 M. M. Mandoc, L. J. A. Koster and P. W. M. Blom, *Appl. Phys. Lett.*, 2007, **90**, 133504.
49 L. J. A. Koster, V. D. Mihailetchi and P. W. M. Blom, *Appl. Phys. Lett.*, 2006, **88**, 052104.
50 J. C. Blakesley and D. Neher, *Phys. Rev. B: Condens. Matter Mater. Phys.*, 2011, **84**, 075210.
51 C. Deibel, A. Wagenpfahl and V. Dyakonov, *Phys. Status Solidi RRL*, 2008, **2**, 175.
52 A. Wagenpfahl, C. Deibel and V. Dyakonov, *IEEE J. Sel. Top. Quantum Electron.*, 2010, **16**, 1759.
53 J. D. Servaites, M. A. Ratner and T. J. Marks, *Appl. Phys. Lett.*, 2009, **95**, 163302.
54 M. Zhang, H. Wang and C. W. Tang, *Appl. Phys. Lett.*, 2010, **97**, 143503.

55 J. C. Wang, X. C. Ren, S. Q. Shi, C. W. Leung and P. K. L. Chan, *Org. Electron.*, 2011, **12**, 880.
56 A. Wagenpfahl, D. Rauh, M. Binder, C. Deibel and V. Dyakonov, *Phys. Rev. B: Condens. Matter Mater. Phys.*, 2010, **82**, 115306.
57 M. Zhang, H. Wang and C. W. Tang, *Appl. Phys. Lett.*, 2011, **99**, 213506.
58 J. Wagner, M. Gruber, A. Wilke, Y. Tanaka, K. Topczak, A. Steindamm, U. Hörmann, A. Opitz, Y. Nakayama, H. Ishii, J. Pflaum, N. Koch and W. Brütting, *J. Appl. Phys.*, 2012, **111**, 054509.
59 B. Ecker, H.-J. Egelhaaf, R. Steim, J. Parisi and E. von Hauff, *J. Phys. Chem. C*, 2012, **116**, 16333.
60 M. Vogel, S. Doka, Ch. Breyer, M. Ch. Lux-Steiner and K. Fostiropoulos, *Appl. Phys. Lett.*, 2006, **89**, 163501.
61 D. Credgington, R. Hamilton, P. Atienzar, J. Nelson and J. R. Durrant, *Adv. Funct. Mater.*, 2011, **21**, 2744.
62 H. Jin, M. Tuomikoski, J. Hiltunen, P. Kopola, A. Maaninen and F. Pino, *J. Phys. Chem. C*, 2009, **113**, 16807.
63 B. T. de Villers, C. J. Tassone, S. H. Tolbert and B. J. Schwartz, *J. Phys. Chem. C*, 2009, **113**, 18978.
64 T. Stubhan, N. Li, N. A. Luechinger, S. C. Halim, G. J. Matt and C. J. Brabec, *Adv. Energy Mater.*, 2012, **2**, 1433.
65 T. Stubhan, M. Salinas, A. Ebel, F. C. Krebs, A. Hirsch, M. Halik and C. J. Brabec, *Adv. Energy Mater.*, 2012, **2**, 532.
66 T. Stubhan, T. Ameri, M. Salinas, J. Krantz, F. Machui, M. Halik and C. J. Brabec, *Appl. Phys. Lett.*, 2011, **98**, 253308.
67 M. D. Irwin, D. B. Buchholz, A. W. Hains, R. P. H. Chang and T. J. Marks, *Proc. Natl. Acad. Sci. U. S. A.*, 2008, **105**, 2783.
68 C. Tao, S. Ruan, G. Xie, X. Kong, L. Shen, F. Meng, C. Liu, X. Zhang, W. Dong and W. Chen, *Appl. Phys. Lett.*, 2009, **94**, 043311.
69 B. P. Rand, J. Li, J. Xue, R. J. Holmes, M. E. Thompson and S. R. Forrest, *Adv. Mater.*, 2005, **17**, 2714.
70 P. Peumans, V. Bulović and S. R. Forrest, *Appl. Phys. Lett.*, 2000, **76**, 2650.
71 J. Wagner, M. Gruber, A. Hinderhofer, A. Wilke, B. Bröker, J. Frisch, P. Amsalem, A. Vollmer, A. Opitz, N. Koch, F. Schreiber and W. Brütting, *Adv. Funct. Mater.*, 2010, **20**, 4295.
72 R. F. Salzman, J. Xue, B. P. Rand, A. Alexander, M. E. Thompson and S. R. Forrest, *Org. Electron.*, 2005, **6**, 242.
73 S. Lacic and O. Inganäs, *J. Appl. Phys.*, 2005, **97**, 124901.
74 A. M. Ballantyne, L. Chen, J. Dane, T. Hammant, F. M. Braun, M. Heeney, W. Duffy, I. McCulloch, D. D. C. Bradley and J. Nelson, *Adv. Funct. Mater.*, 2008, **18**, 2373.
75 C. Müller, E. Wang, L. M. Andersson, K. Tvingstedt, Y. Zhou, M. R. Andersson and O. Inganäs, *Adv. Funct. Mater.*, 2010, **20**, 2124.
76 R. Pandey and R. J. Holmes, *Appl. Phys. Lett.*, 2012, **100**, 083303.
77 A. J. Moulé, J. B. Bonekamp and K. Meerholz, *J. Appl. Phys.*, 2006, **100**, 094503.
78 A. Gadisa, F. Zhang, D. Sharma, M. Svensson, M. R. Adnersson and O. Inganäs, *Thin Solid Films*, 2007, **515**, 3126.
79 B. Ray, P. R. Nair and M. A. Alam, *Sol. Energy Mater. Sol. Cells*, 2011, **95**, 3287.
80 B. Ray and M. A. Alam, *Sol. Energy Mater. Sol. Cells*, 2012, **99**, 204.
81 L. Onsager, *Phys. Rev.*, 1938, **54**, 554.
82 C. L. Braun, *J. Chem. Phys.*, 1984, **80**, 4157.
83 W. Tress, K. Leo and M. Riede, *Adv. Funct. Mater.*, 2011, **21**, 2140.
84 Y. Shen, K. Li, N. Majumdar, J. C. Campbell and M. C. Gupta, *Sol. Energy Mater. Sol. Cells*, 2011, **95**, 2314.
85 T. Aeronouts, W. Greens, J. Poortmans, S. Borghs and R. Mertens, *Thin Solid Films*, 2002, **403–404**, 297.
86 S. Dongaonkar, J. D. Servaites, G. M. Ford, S. Loser, J. Moore, R. M. Gelfand, H. Mohseni, H. W. Hillhouse, R. Agrawal, M. A. Ratner, T. J. Marks, M. S. Lundstrom and M. A. Alam, *J. Appl. Phys.*, 2010, **108**, 124509.
87 A. M. Goodman and A. Rose, *J. Appl. Phys.*, 1971, **42**, 2823.
88 M. M. Mandoc, W. Veurman, L. J. A. Koster, B. de Boer and P. W. M. Blom, *Adv. Funct. Mater.*, 2007, **17**, 2167.
89 Y. Zhang, X.-D. Dang, C. Kim and T.-Q. Nguyen, *Adv. Energy Mater.*, 2011, **1**, 610.
90 R. Mauer, I. A. Howard and F. Laquai, *J. Phys. Chem. Lett.*, 2010, **1**, 3500.
91 B. Muhsin, J. Renz, K.-H. Drüe, G. Gobsch and H. Hoppe, *Phys. Status Solidi A*, 2009, **206**, 2771.
92 P. Peumans and S. R. Forrest, *Chem. Phys. Lett.*, 2004, **398**, 27.
93 D. M. Stevens, J. C. Speros, M. A. Hillmyer and C. D. Frisbie, *J. Phys. Chem. C*, 2011, **115**, 20806.
94 C. G. Shuttle, R. Hamilton, B. C. O'Regan, J. Nelson and J. R. Durrant, *Proc. Natl. Acad. Sci. U. S. A.*, 2010, **107**, 16448.
95 M. Lenes, L. J. A. Koster, V. D. Mihailetchi and P. W. M. Blom, *Appl. Phys. Lett.*, 2006, **88**, 243502.
96 V. D. Mihailetchi, H. Xie, B. de Boer, L. J. A. Koster and P. W. M. Blom, *Adv. Funct. Mater.*, 2006, **16**, 699.
97 A. Kumar, S. Sista and Y. Yang, *J. Appl. Phys.*, 2009, **105**, 094512.
98 C. Uhrich, D. Wynands, S. Olthof, M. K. Riede, K. Leo, S. Sonntag, B. Maennig and M. Pfeiffer, *J. Appl. Phys.*, 2008, **104**, 043107.

